J. Fluid Mech. (1975), *vol.* 69, *part* 1, *pp.* 129–144
Printed in Great Britain

The development of weak waves in the unsteady one-dimensional flow of a vibrationally relaxing gas ahead of an impulsively started piston

By C. G. DAIN† AND J. P. HODGSON
Department of the Mechanics of Fluids, University of Manchester, England

(Received 16 September 1974)

The method of characteristics is used to calculate the flow ahead of an impulsively started piston moving at constant velocity. Particular attention is paid to the development of weak shock waves which are either fully or partly dispersed at very large distances from the piston. It is found that the global features of the flows may be represented in similarity form, and the graphs obtained allow extrapolation to very weak waves.

1. Introduction

The flows described in this paper are the one-dimensional unsteady analogues of the two-dimensional steady flows discussed in the preceding paper by Hornby & Johannesen (1975). The two projects were carried out simultaneously and although some descriptions are necessarily similar to those of Hornby & Johannesen, it is intended that the reports be complementary as far as certain details are concerned.

When an impulsively started piston moves into an inviscid relaxing gas which is initially at rest and in equilibrium the gas is set in motion by a shock wave which moves ahead of the piston. A schematic diagram of the flow in the x, t plane is shown in figure 1. The passage of the shock wave creates non-equilibrium thermodynamic states within the gas and equilibrium is achieved by relaxation of the various energy modes of the gas molecules. The relaxation processes modify the structure of the shock wave as it progresses and eventually the shock wave attains a stable structure moving at constant velocity. In this paper the particular non-equilibrium phenomenon of interest is vibrational relaxation of a pure gas, but the qualitative features of these flows are typical of similar flows in gases exhibiting other types of relaxation. The rotational and translational energy modes are assumed to be in local equilibrium throughout. Viscosity and heat conduction are neglected.

The gas at the piston surface attains the piston velocity instantaneously, being accelerated by a frozen shock across which the vibrational energy remains unchanged. The frozen shock may be considered to be a mathematical discontinuity. Behind the frozen shock a state of non-equilibrium exists. The

† Present address: Logica Limited, 31–36 Foley Street, London W1P 7LB.

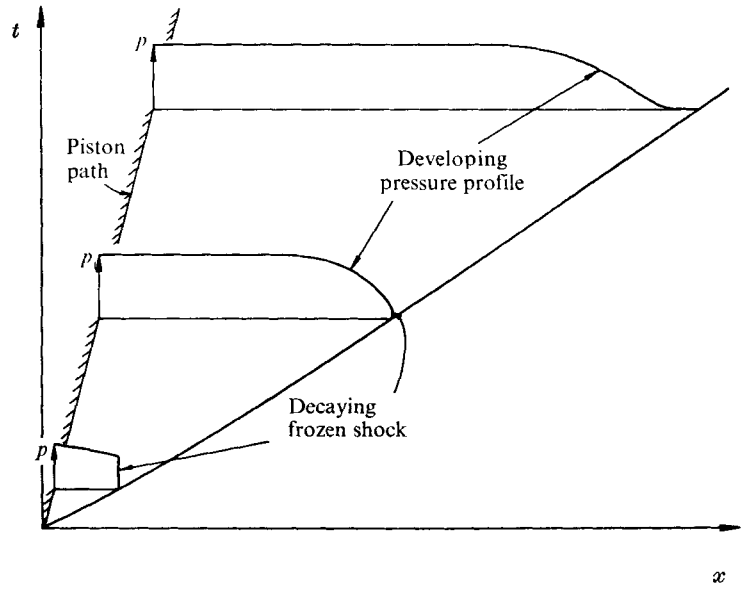

FIGURE 1. Schematic diagram of the flow ahead of an impulsively started piston leading to a fully dispersed shock wave at infinity, i.e. $x, t \to \infty$.

subsequent vibrational relaxation causes the frozen shock to decay, and a relaxation region develops behind it. The gas is accelerated to the piston speed through the weakened frozen shock and the relaxation region. Eventually equilibrium conditions are achieved at the piston and the region of non-equilibrium is localized behind the frozen shock. The shock wave (frozen shock and relaxation region) finally acquires the thermodynamic structure of a steady wave moving at constant velocity with strength sufficient to accelerate the gas to the piston velocity. In a co-ordinate system fixed in this wave the flow is steady and the structure of such waves has been discussed in detail in the literature, notably by Lighthill (1956). Knowledge of the final wave structure allows a detailed check on the accuracy of any method used to calculate the entire flow. The final wave structure in the unsteady problem under investigation occurs at infinity in both the distance and time co-ordinates and will be referred to as the wave at infinity. This wave may be fully or partly dispersed depending on the speed of the piston and on the vibrational specific-heat contribution to the undisturbed gas. The actual line in the x, t diagram along which the wave at infinity lies is not known *a priori*. For a fully dispersed wave the frozen shock decays to zero strength. Of particular interest are the length scales over which the shock wave must travel as it develops its final structure, and we concentrate on the development of fully dispersed and weak, partly dispersed waves.

There are various analytical approaches to the problem in the literature. The linearized theory of wave propagation in a relaxing gas has been given, for example, by Clarke (1960), Moore & Gibson (1960) and Lick (1967). The linearized expression for the decay distance of the frozen shock is given in the appendix and

used later to normalize the numerical results. Nonlinear theories have been developed by Blythe (1969) and Ockendon & Spence (1969). Both papers present analytic results based on approximations involving small vibrational specific heat and/or small or even smaller piston speed (both suitably non-dimensionalized). One of the difficulties in interpreting their results is that it is not clear how large a particular small quantity may be before the various approximations cease to be valid. Ockendon & Spence restricted their considerations to a piston having finite acceleration, introducing a second length scale into the problem but avoiding the appearance of a frozen shock. Blythe obtained a similarity solution in functional form for the present problem with small piston speed and small vibrational specific heat. In the present paper no analytical approximations are made and the equations are solved using the method of characteristics.

It has been established by Hodgson & Johannesen (1971) that vibrational relaxation of the constituents of the atmosphere may be responsible for the dispersion of sonic-bang shock waves. The development of the wave is of critical significance in determining the extent to which the steady wave profile is valid.

2. Calculation procedure

The calculations are based on a characteristic network, step-by-step procedure combined with the shock relations for the frozen shock. Using the heat-transfer analogy explained by Johannesen, Bird & Zienkiewicz (1967), in which the flow is treated as if it were an ideal-gas flow with heat extraction equal to the increase in vibrational energy, formulation of the equations is straightforward.

The non-dimensionalization is similar to that given by Hornby & Johannesen. A prime indicates dimensional quantities and all unprimed variables are non-dimensional:

$$p' = p'_\infty p, \quad \rho' = \rho'_\infty \rho, \quad T' = T'_\infty T, \tag{1)–(3}$$

$$(u', a') = (R'T'_\infty)^{\frac{1}{2}}(u, a), \tag{4}$$

$$(c'_p, c'_{\text{vib}}, s') = R'(c_p, c_{\text{vib}}, s), \tag{5}$$

$$\sigma' = R'T'_\infty \sigma, \quad \Phi' = \Phi'_\infty \Phi, \tag{6), (7}$$

$$x' = \frac{(R'T'_\infty)^{\frac{1}{2}}}{\rho'_\infty \Phi'_\infty} x, \quad t' = \frac{1}{\rho'_\infty \Phi'_\infty} t. \tag{8), (9}$$

A suffix ∞ denotes conditions in the undisturbed gas ahead of the wave. p', ρ' and T' are the pressure, density and translational temperature, u' is the velocity, a' the frozen speed of sound, R' the gas constant, c'_p the frozen specific heat at constant pressure, c'_{vib} the vibrational specific heat, s' the entropy, σ' the vibrational energy, Φ' the relaxation frequency, x' the distance and t' the time measured from the start of the motion of the piston.

Φ is defined by the well-known relaxation equation

$$D\sigma/Dt = \rho\Phi(\bar{\sigma} - \sigma), \tag{10}$$

where $\bar{\sigma}$ is the local equilibrium value of the vibrational energy and a function of temperature only. The characteristics equations describing the flow are

$$dx/dt = u + a \tag{11}$$

for the C^+ characteristics, along which

$$dp+\rho a\,du = -(\gamma-1)\rho^2\Phi(\bar{\sigma}-\sigma)\,dt, \tag{12}$$

$$dx/dt = u-a \tag{13}$$

for the C^- characteristics, along which

$$dp-\rho a\,du = -(\gamma-1)\rho^2\Phi(\bar{\sigma}-\sigma)\,dt, \tag{14}$$

and

$$dx/dt = u \tag{15}$$

for the particle paths, along which

$$dp-a^2\,d\rho = -(\gamma-1)\rho^2\Phi(\bar{\sigma}-\sigma)\,dt, \tag{16}$$

where γ is the ratio of the principal specific heats. Throughout the flow the thermal equation of state is valid, i.e.

$$p = \rho T. \tag{17}$$

Equations (11)–(17) were used to calculate the flow.

There are two boundary conditions: (i) at the piston $u = u_P$, the velocity of the piston, and (ii) the conditions immediately behind the frozen shock are matched to those of the undisturbed gas by the frozen shock relations. At the origin the flow velocity behind the frozen shock is equal to the piston velocity, so that the frozen shock is known there.

To proceed with the numerical calculation we require the functional relationships $\bar{\sigma} = \bar{\sigma}(T)$ and $\Phi = \Phi(T)$. Since we are interested in flows which have small temperature variations it has been assumed that

$$\bar{\sigma} = \bar{\sigma}_\infty + c_{\text{vib}}(T-1), \tag{18}$$

where c_{vib} is a constant for a particular flow, and that

$$\Phi = 1. \tag{19}$$

It is straightforward to include the actual temperature dependences for a particular gas. For the flows considered the effect of doing this would be small and the results would be more difficult to apply generally.

Each flow is then determined by three parameters: the frozen specific-heat ratio γ, the vibrational specific heat c_{vib} and the piston speed u_P. Twenty-one flows were calculated using $\gamma = \frac{7}{5}$ and $c_{\text{vib}} = 0{\cdot}5$, 1 and 2 with $u_P < 0{\cdot}14$.

The network was based on the C^+ and C^- characteristics with interpolation along the particle paths through each network point. The flow was calculated in the x, t plane and retains the advantages of easy physical interpretation. The network was built up in a series of layers by starting each layer at the piston and proceeding along the C^+ characteristic to the frozen shock. Within each network element the usual methods of iteration, discussed by Sedney (1970), were employed for higher accuracy. When the frozen shock was reached at the end of each layer its strength was determined by applying the differential frozen shock relations along the shock path from the last point of the preceding layer.

The form of the relaxation equation (10) indicates that equilibrium is approached asymptotically as $t\to\infty$, and in the flows considered the largest

departure from equilibrium occurs at the origin, where the frozen shock is strongest. It follows that if steps corresponding to constant time intervals along the piston path are taken to define each new layer of the network (this would be the usual approach) the greatest errors occur in the first layer, which is in fact a single triangle. Further, a prohibitively large number of steps is subsequently required to obtain details of the flow in the far field. An alternative is to increase the step size along the piston path as the calculation proceeds. The relaxation equation provides a clue as to how this should be done. The interval between adjacent C^+ characteristics at the piston was chosen such that the same change in σ occurred between them. The step size measured in terms of time increased along the piston path, with smaller steps occurring where the thermodynamic gradients were large. It was thus possible to progress much further into the flow with greater efficiency. However, the step size cannot be increased indefinitely as the details of the developing wave structure would eventually become embedded in a single layer of the network. To avoid this, steps corresponding to constant time intervals were used when the gas at the piston was getting close to equilibrium. The magnitude of the 'constant-t' steps was made equal to that of the last of the 'constant-σ' steps, and the detailed structure of the wave was obtained.

For flows which lead to a wave at infinity which is fully dispersed the frozen shock decays to zero strength before the calculation is complete. In practice the shock strength became negative, and the shock was then replaced by a C^+ characteristic in the undisturbed gas ahead of the wave. This procedure was no less accurate than any other network point calculation. A running check, suggested by Zhukov (1960), was made on the results by integrating the continuity, momentum and energy equations from the origin along the piston and C^+ characteristics to the frozen shock. Such integration is almost certainly in greater error than the characteristics calculations themselves, but nevertheless the equations were found to be satisfied to within one part in 10^4 per unit distance from the origin.

For all flows the structure of the wave at infinity is known from one-dimensional steady flow considerations. The structure can be obtained as profiles along the characteristics in the x, t plane for a wave moving into a gas at rest, and the developing wave profiles can be readily compared with the independently calculated profile of the wave at infinity. In practice, profiles of σ and $\bar{\sigma}-\sigma$ projected along C^- characteristics were used since this family traverses the wave much more rapidly than the C^+ characteristics.

The calculation procedure is illustrated by the flow for which $u_P/a_\infty = 0{\cdot}08$ and $c_{\mathrm{vib}} = 2$. These values lead to a fully dispersed wave at infinity.

For very small times the flow may be calculated analytically from the initial gradients, which are given in the appendix. These initial gradients are independent of the detailed numerical procedure used for calculating the entire flow.

The constant-σ step size along the piston was defined in terms of a certain fraction of $(\bar{\sigma}-\sigma)_0$, where the suffix 0 denotes conditions behind the frozen shock at the origin. For early calculations different fractions were used to investigate the effects of varying the step size, but in the majority of the calculations the

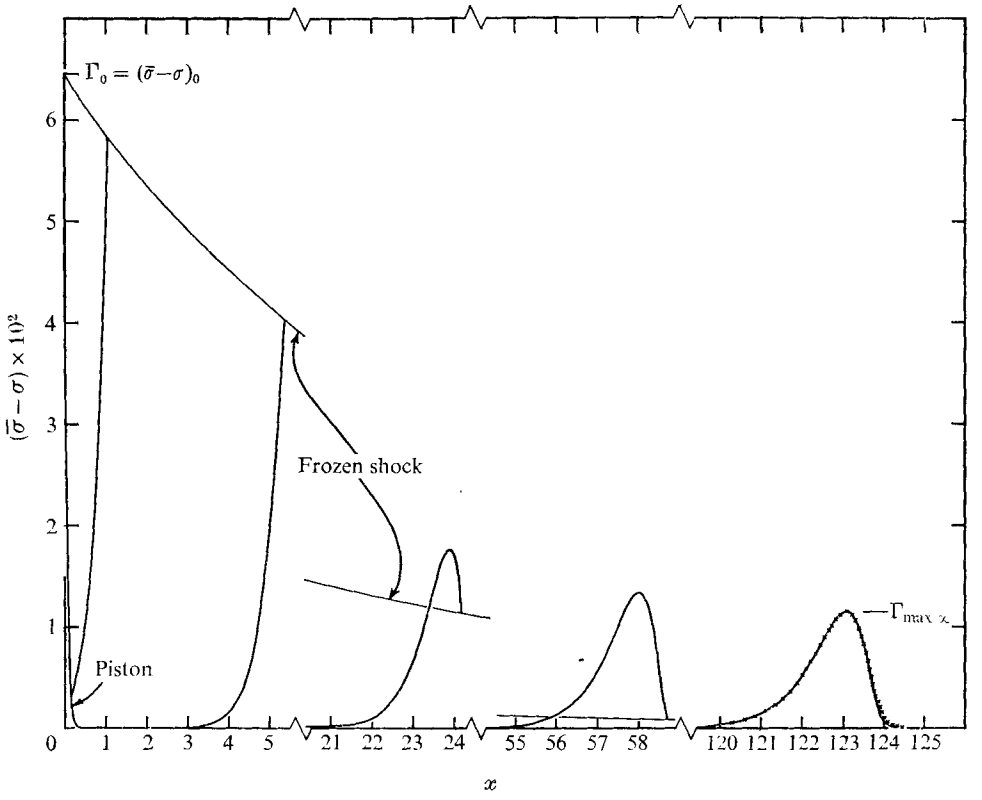

FIGURE 2. Profiles of the departure from equilibrium along selected C^- characteristics, showing how the wave profile develops towards the profile of the wave at infinity, which is represented by crosses. The departure from equilibrium at the piston and frozen shock is also indicated.

change in σ was $\frac{1}{50}(\bar{\sigma}-\sigma)_0$. The changeover to constant steps was made when $\bar{\sigma}-\sigma$ at the piston was about $\frac{1}{10}(\bar{\sigma}-\sigma)_0$, and subsequent steps along the piston path were about ten times the initial step.

At the piston it was found that $\bar{\sigma}-\sigma$ approached zero indistinguishably from an exponential function of time, i.e.

$$(\bar{\sigma}-\sigma)_P = (\bar{\sigma}-\sigma)_0 \exp(-t/t_P), \tag{20}$$

where the suffix P denotes conditions at the piston and t_P is the characteristic time for the achievement of equilibrium at the piston. t_P may be obtained analytically from the initial gradients and is given by equation (A 13) in the appendix.

The greatest departure from equilibrium occurs at the origin, and the gas at the piston relaxes to equilibrium with the greatest entropy increase in the entire flow. At the origin the frozen shock is strongest and the entropy increase through it is almost identical to the entropy increase through the wave at infinity, being of order u_P^3 for $u_P \ll 1$. Using arguments similar to those of Hornby & Johannesen it can be shown that the entropy increase at the piston due to relaxation is of order u_P^2. There is a gradual decrease of entropy with increasing distance from the

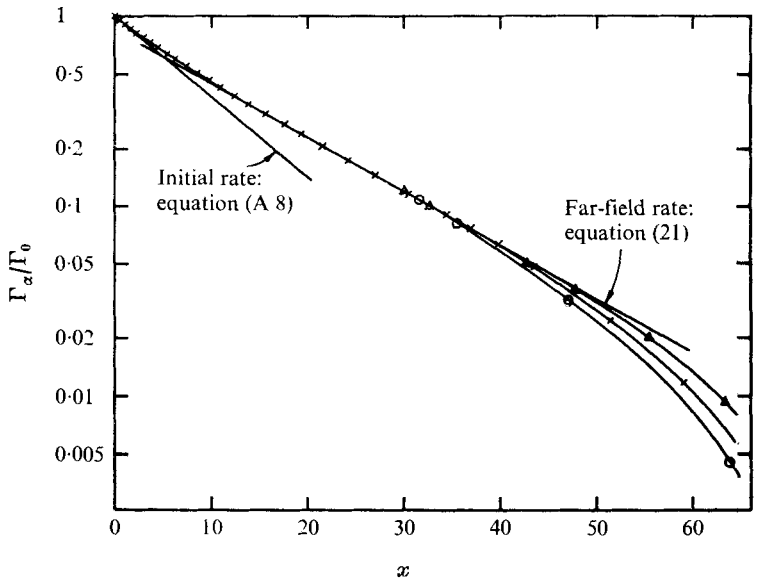

FIGURE 3. Decay of the frozen shock represented by the departure from equilibrium behind it. $u_P/a_\infty = 0{\cdot}08$, $c_{vib} = 2$ and $\gamma = \frac{7}{5}$. ○, $\frac{1}{25}$ steps; ×, $\frac{1}{50}$ steps; △, $\frac{1}{100}$ steps.

piston and the thickness of the 'entropy layer' is of the same order as the development distance of the wave.

Of greater interest are the decay of the frozen shock and the evolution of the wave towards its structure at infinity. For the example, the development of the wave is illustrated in figure 2, where $\bar{\sigma}-\sigma$ is plotted against x along selected C^- characteristics. The decay of the frozen shock is indicated and it was replaced by a C^+ characteristic at $x = 68{\cdot}0$. The calculation was continued until the developing $\bar{\sigma}-\sigma$ profile was almost indistinguishable from the profile at infinity.

The two main features of the evolution of the wave are the decay of the frozen shock and the development of the wave structure. Both are analysed further by considering the local departure $\Gamma = \bar{\sigma}-\sigma$ from equilibrium. The frozen shock decay is represented by plotting

$$(\Gamma_\alpha - \Gamma_{\alpha\infty})/(\Gamma_0 - \Gamma_{\alpha\infty})$$

against x, where the suffix α denotes conditions behind the frozen shock and the suffix ∞ the conditions in the wave at infinity. If the wave at infinity is fully dispersed, as in the example, then $\Gamma_{\alpha\infty} = 0$. The shock wave development is represented by plotting

$$(\Gamma_{max} - \Gamma_{max\infty})/(\Gamma_0 - \Gamma_{max\infty})$$

against x, where Γ_{max} is the maximum departure from equilibrium along a C^- characteristic and $\Gamma_{max\infty}$ is the maximum departure from equilibrium in the wave at infinity. Initially Γ_{max} coincides with Γ_α but as the frozen shock decays Γ_{max} occurs some distance behind the frozen shock (see figure 2). For large values of u_P, Γ_{max} and Γ_α coincide throughout the evolution of the wave.

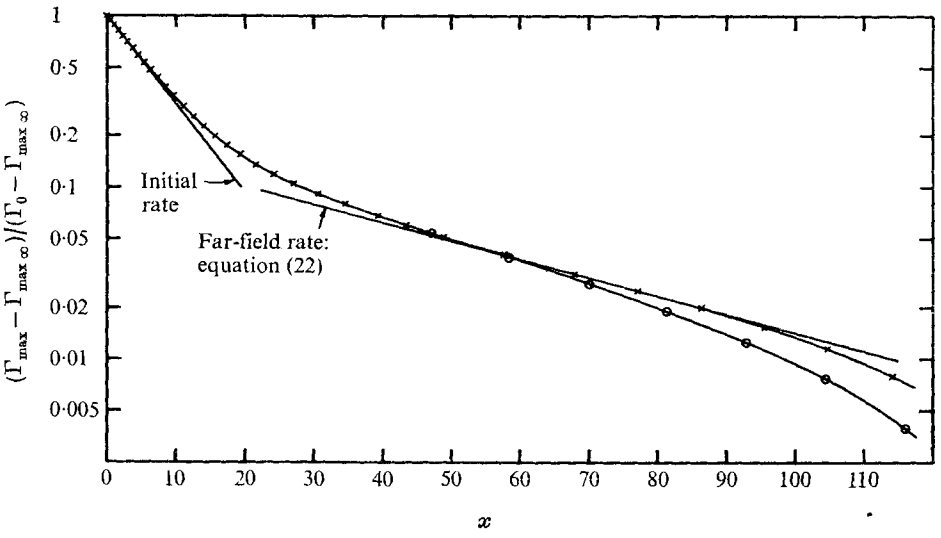

FIGURE 4. Shock wave development for profiles along C^- characteristics. $u_P/a_\infty = 0{\cdot}08$, $c_{vib} = 2$ and $\gamma = \frac{7}{5}$. ○, $\frac{1}{25}$ steps; ×, $\frac{1}{50}$ steps.

The frozen shock decay is illustrated in figure 3. The results show that, for the three different step sizes used, there is no difference between the decay curves until the strength of the frozen shock is less than about 10 % of its initial value. However, after that the largest step size indicates the most rapid decay. Since the calculations for the smallest step size are expected to be most accurate, the indications are that the decay of the frozen shock at large distances can be represented by the equation

$$\Gamma_\alpha/\Gamma_0 = A\exp(-x/x_\alpha), \tag{21}$$

which is a straight line on the logarithmic plot of figure 3. Here A is the value of Γ_α/Γ_0 obtained by extending the line on figure 3 to the intersection with $x = 0$, and x_α is the far-field decay distance for the frozen shock. The near field may be represented by the initial gradient given by equation (A 8) in the appendix. The initial decay rate is always greater than the far-field decay rate and there is a gradual change in the local decay rate between the two extremes.

The shock wave development is illustrated in figure 4. Again there are two characteristic rates of development in the near and far fields. The results for the larger step size indicate a more rapid development in the far field but those for the smaller step size are expected to be more accurate. The far-field wave development may be represented by the equation

$$(\Gamma_{max} - \Gamma_{max\infty})/(\Gamma_0 - \Gamma_{max\infty}) = B\exp(-x/x_\beta), \tag{22}$$

where B is the value of $(\Gamma_{max} - \Gamma_{max\infty})/(\Gamma_0 - \Gamma_{max\infty})$ obtained by extending the straight line on figure 4 to $x = 0$, and x_β is the far-field shock wave development distance. The near field is represented by the initial gradient, calculated using results obtained in the appendix and the equations defining the wave at infinity.

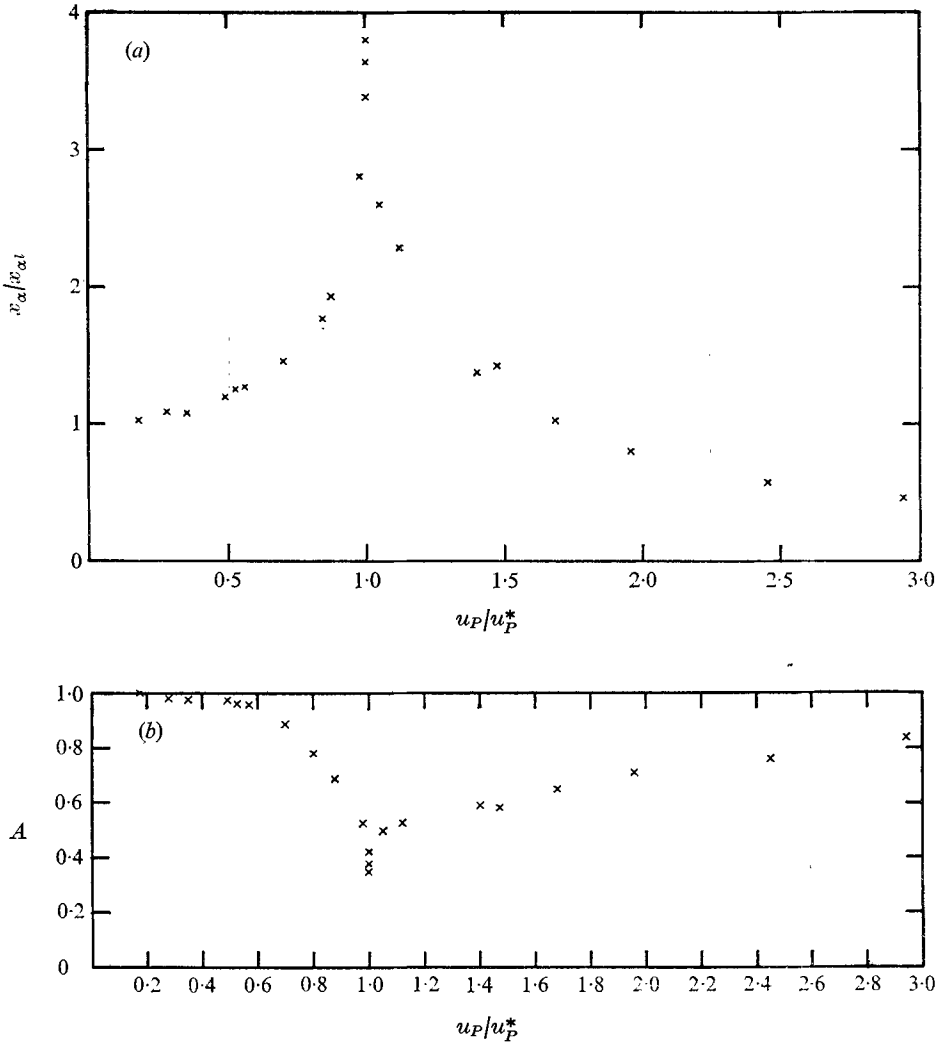

FIGURES 5 (*a*, *b*). For legend see next page.

In the general calculations (21) and (22) were the tangents to the curves of figures 3 and 4 obtained using constant-σ steps of $\frac{1}{50}(\bar{\sigma}-\sigma)_0$ at the point of maximum slope. Graphs of this type were plotted for all flows calculated and further reduction of the results was based on a study of the four constants x_α, A, x_β and B.

3. Comparison of the properties of various flows

The results described in §2 were obtained for gases with $c_{\text{vib}} = 0{\cdot}5$, 1 and 2 and piston speeds in the range $0{\cdot}02 < u_P < 0{\cdot}14$. In all cases considered the near-field flow was adequately described by the initial gradients given in the appendix. The gas properties at the piston were also described by the initial gradients since the

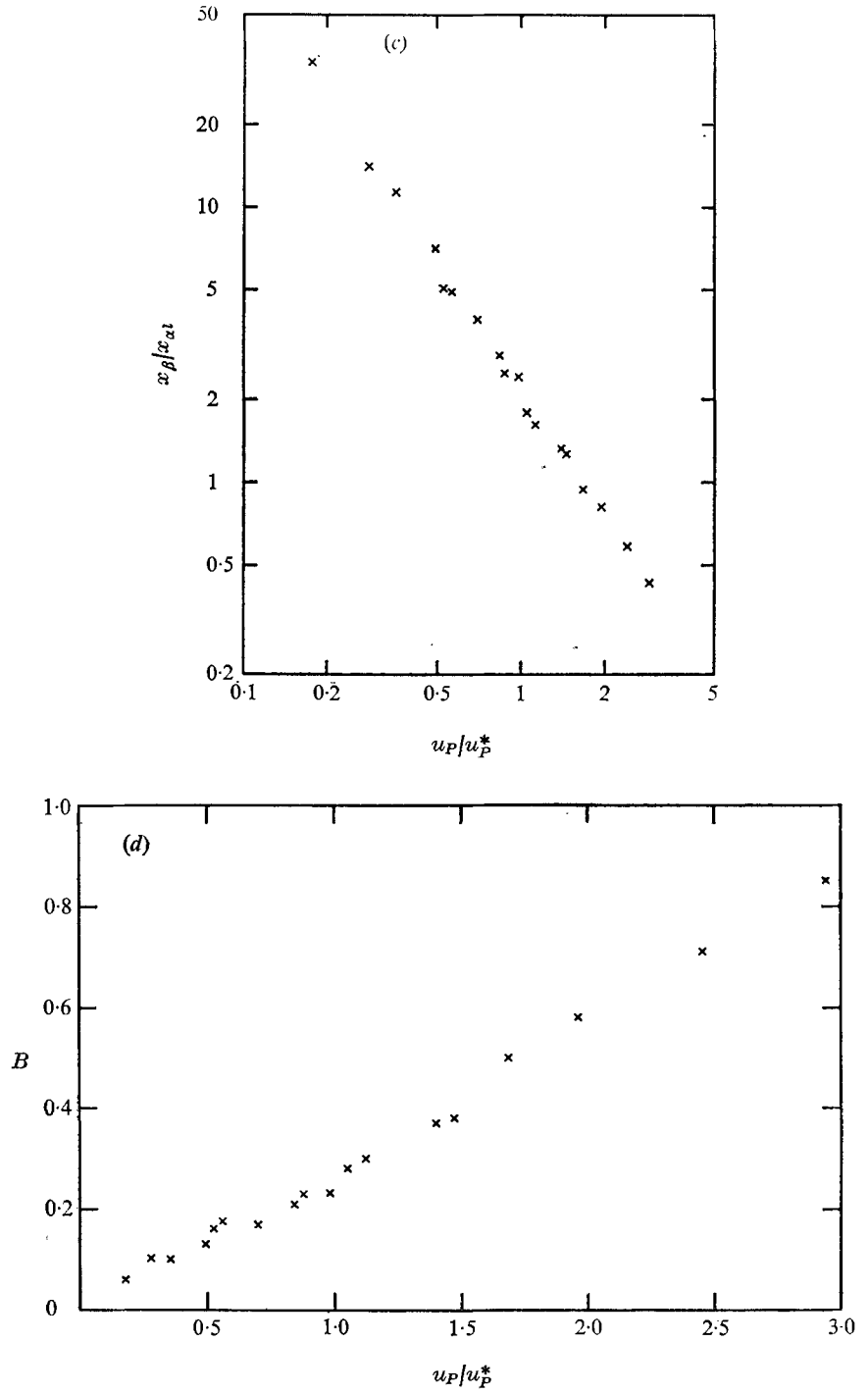

FIGURE 5. Normalized plots of (*a*) the far-field frozen shock decay distance, (*b*) the value of A defined by (21), (*c*) the far-field shock wave development distance and (*d*) the value of B defined by (22).

departure from equilibrium at the piston approached zero exponentially with time according to (20). The far-field behaviour of the flow concerns the frozen shock decay, which is characterized by x_α and A, and the shock wave development, characterized by x_β and B. These four quantities were plotted against u_P for various values of c_{vib}. The form of the graphs indicated that, with suitable normalization, a universal curve might exist for each quantity.

If the piston speed u_P was normalized by u_P^*, the piston speed which leads to the strongest possible fully dispersed wave at infinity, the values of A and B collapsed onto single curves. If, in addition, the values of x_α and x_β were normalized by $x_{\alpha l}$, the frozen shock decay distance for infinitely small piston speed, they also collapsed onto single curves. $x_{\alpha l}$ is usually derived from the linearized equations of motion but a simple derivation from the initial gradients is included in the appendix, with the result given by equation (A 14).

For the far-field frozen shock decay $x_\alpha/x_{\alpha l}$ and A are plotted against u_P/u_P^* in figures 5 (*a*) and (*b*). The scatter on these graphs is within the computational accuracy. As $u_P \to 0$, $x_\alpha \to x_{\alpha l}$, indicating that the results are consistent with linearized theory. For $u_P = u_P^*$, the far-field frozen shock decay distance has a maximum equal to about 3·5 times the linearized value. The physical reason for the maximum is that the maximum-strength fully dispersed wave travels at the frozen sound speed in the undisturbed gas and the C^+ characteristics from the piston travel at the local frozen sound speed. At the front of a maximum-strength fully dispersed wave the C^+ characteristics become asymptotically coincident with the front of the wave, and information propagated from the piston takes a long time to reach the wave front. These results for $u_P = u_P^*$ are also the most difficult to calculate, since the characteristic network elements near the wave front become elongated in the direction of the wave, and they probably contain the greatest computational errors.

For the far-field shock wave development $x_\beta/x_{\alpha l}$ and B are plotted in figures 5 (*c*) and (*d*). The graphs indicate the same trends as figures 6 (*c*) and (*d*) in the previous paper by Hornby & Johannesen. The far-field wave development distance may be determined from the empirical equation

$$x_\beta/x_{\alpha l} = 2{\cdot}0(u_P/u_P^*)^{-1{\cdot}6} \tag{23}$$

and the development distances are greatest for small piston speeds. Since the width of the wave at infinity is inversely proportional to its strength, the C^+ characteristics require a longer time to traverse the developing wave if it is weak. This statement is not inconsistent with the above comments concerning the frozen shock, since for weak fully dispersed waves at infinity the frozen shock decays to zero strength long before the developing wave attains a structure remotely similar to that of the wave at infinity. From figure 5 (*c*) the value of the empirical parameter B is given by

$$B = 0{\cdot}27u_P/u_P^*. \tag{24}$$

The numerical values are based on the results of both investigations.

The plotted points of figures 5 (*a*) and (*b*) do not lend themselves to simple curve-fitting techniques.

4. Conclusions

The results presented indicate that the flow near the origin of the motion of an impulsively started piston can be well represented by the thermodynamic gradients at the origin. Further, the departure from equilibrium at the piston approaches zero exponentially at a rate defined by the initial gradient of $\bar{\sigma} - \sigma$.

The far-field wave evolution can be grossly represented in terms of four universal curves which describe the frozen shock decay and shock wave development. Linking the piston speed to the properties of the undisturbed gas, via the piston speed which leads to a maximum-strength fully dispersed wave at infinity, allows flows for all possible combinations of piston speed and vibrational specific heat to be predicted.

To obtain the numerical solutions the characteristics network was built up in a systematic manner with small step sizes in the x, t plane occurring in the region of the flow where the thermodynamic gradients were largest. This permitted the flow to be efficiently evaluated at large distances and times.

A similarity solution for the flow ahead of an impulsively started piston was obtained by Blythe for $c_{\text{vib}} \ll 1$ and $u_P \ll 1$. His solution, which is in functional form only, is compatible with the similarity of the characteristics results, for which $c_{\text{vib}} = 0{\cdot}5$, 1 or 2. The characteristics solutions are in a form which may be readily used to determine the gross features of all flows of this type. The graphs plotted in figure 5 are identical, to within the computational error, to those plotted in figure 6 of the previous paper by Hornby & Johannesen. It is thus apparent that, not only is there similarity within each type of flow, but there is also similarity between the two types. The normalizations of the piston speed and wedge angle were the same in both cases, based on the values leading to a maximum-strength fully dispersed shock wave at infinity. The normalizations of the decay and development distances were also the same in both cases, provided that the distances for decay and development in the two-dimensional steady flow were measured from the wedge to the wave in a direction normal to the wave. In the acoustically linearized limit this is accounted for by the factor $M_\infty/(M_\infty^2 - 1)^{\frac{1}{2}}$, which transforms y into the distance normal to the wave.

In spite of the fact that in all cases the piston speed and wave angle were not large, it does not appear that this is the usual form of the analogy between one-dimensional unsteady and two-dimensional steady flows. Rather, it is the analogy between one-dimensional unsteady and two-dimensional unsteady flows since $y(M_\infty^2 - 1)^{\frac{1}{2}}/M_\infty$ is the distance the wave has travelled since its creation at the tip of the wedge. Thus the lifetime of the wave as it moves into the gas ahead of it is the criterion which determines its structure.

A similarity solution for the two-dimensional steady flow past a wedge was also obtained by Blythe for $c_{\text{vib}} \ll 1$ and $\theta_w \ll 1$. His solution indicates the same type of similarity as that obtained by Hornby & Johannesen.

The results obtained by the method of characteristics show that the frozen shock decay distance differs substantially from that obtained from linearized theory. Blythe's analysis for constant piston speed/wedge angle is able to predict only the linearized frozen shock decay distance in the near field. Presumably

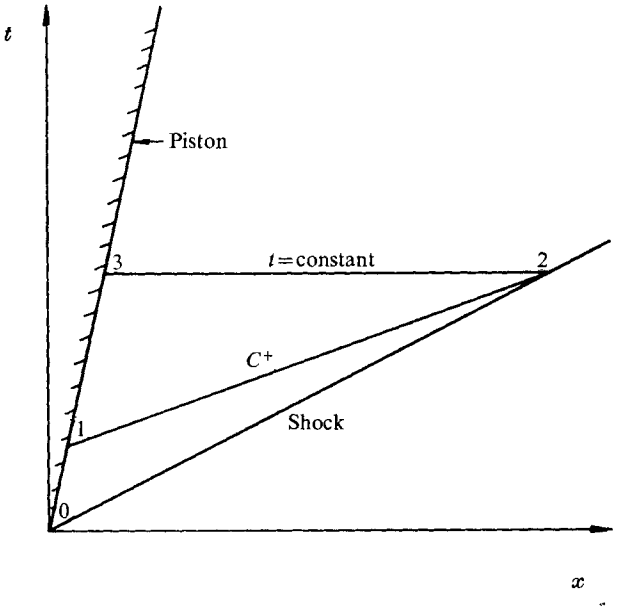

FIGURE 6. Elementary network for obtaining the initial gradients.

this is because, in the limit of small piston speed or wedge angle, the nonlinear effects of the frozen shock are insignificant when compared with those determining the structure of the developing wave.

The characteristics results presented in our two papers give solutions of the exact equations for the flows and are in a form suitable for immediate application to all flows of these types.

We wish to thank Professor N. H. Johannesen and Dr R. P Hornby for many valuable discussions. One of us (C. G. D.) was in receipt of a studentship from the Science Research Council.

Appendix. Calculation of the initial gradients

The initial thermodynamic gradients in the flow ahead of an impulsively started piston moving at constant velocity are most easily derived by considering a C^+ characteristic and a line at constant time in the x, t diagram as shown in figure 6. The line 1–2 is a C^+ characteristic, along which (12) holds:

$$p_2 - p_1 + \rho_0 a_0 (u_2 - u_P) = -(\gamma - 1)\rho_0^2 (\overline{\sigma} - \sigma)_0 (t_2 - t_1), \tag{A 1}$$

where the suffix 0 indicates conditions behind the shock at the origin. Since the piston velocity is constant, the momentum equation along 3–2 reduces to

$$p_3 = p_2. \tag{A 2}$$

Behind a shock moving into a gas at rest

$$p_2 - p_0 = (dp/du)_{u=u_P}(u_2 - u_P), \tag{A 3}$$

where $$\left(\frac{dp}{du}\right)_{u=u_P} = \frac{\gamma+1}{2}u_P + \gamma^{\frac{1}{2}}\left[1+\left(\frac{\gamma+1}{4}\right)^2\frac{u_P^2}{\gamma}\right]^{\frac{1}{2}}.$$

Assuming that the pressure varies linearly at the piston gives

$$(p_3 - p_0)/t_3 = (p_1 - p_0)/t_1. \tag{A 4}$$

The geometry of figure 6 indicates that

$$t_2 = t_3, \quad x_2 = u_{S0}t_2, \quad x_3 = u_P t_3$$

and $$t_1/t_3 = 1 - (u_{S0} - u_P)/a_0,$$

where u_{S0} and u_P are the velocities of the shock and piston, respectively.

Equations (A 1)–(A 4) may be solved for p_1, p_2, p_3 and u_2. The equations defining the geometry then lead to the initial gradients, e.g.

$$\left(\frac{dp}{dx}\right)_{P0} = \frac{p_3 - p_0}{x_3} = -(\gamma-1)\rho_0^2(\bar{\sigma}-\sigma)_0 \Big/ u_P\left[1+\frac{\rho_0 a_0^2}{(u_{S0}-u_P)(dp/du)_{u=u_P}}\right] \tag{A 5}$$

and

$$\left(\frac{dp}{dx}\right)_{S0} = \frac{u_P}{u_{S0}}\left(\frac{dp}{dx}\right)_{P0}, \tag{A 6}$$

where the suffix S denotes conditions behind the frozen shock and the suffix P denotes conditions at the piston. The initial gradients of all other thermodynamic quantities follow. In particular, the departure Γ_α from equilibrium behind the frozen shock has an initial gradient given by

$$\left(\frac{d\Gamma_\alpha}{dx}\right)_{S0} = \left(\frac{d\Gamma_\alpha}{dp}\right)_{S0}\left(\frac{dp}{dx}\right)_{S0},$$

where $$\left(\frac{d\Gamma_\alpha}{dp}\right)_{S0} = \left(\frac{d\bar{\sigma}}{dp}\right)_{S0} = c_{\mathrm{vib}}\left(\frac{dT}{dp}\right)_{S0}.$$

Hence $$\left(\frac{d\Gamma_\alpha}{dp}\right)_{S0} = \frac{c_{\mathrm{vib}}[(\gamma+1)(p_0^2+1)+2(\gamma-1)p_0](\gamma-1)}{[(\gamma+1)p_0+(\gamma-1)]^2}. \tag{A 7}$$

The initial decay rate of the frozen shock represented in figure 3 is therefore given by

$$\left[\frac{d}{dx}\log\left(\frac{\Gamma_\alpha}{\Gamma_0}\right)\right]_0 = -\frac{1}{x_{\alpha 0}} = -\frac{c_{\mathrm{vib}}(\gamma-1)^2\rho_0^2[(\gamma+1)(p_0^2+1)+2(\gamma-1)p_0]}{u_{S0}\left[1+\dfrac{\rho_0 a_0^2}{(u_{S0}-u_P)(dp/du)_{u=u_P}}\right][(\gamma+1)p_0+(\gamma-1)]^2} \tag{A 8}$$

if Γ_α is assumed to behave exponentially near the origin. For partly dispersed waves at infinity $\Gamma_{\alpha\infty}$ must also be calculated to find the corresponding initial decay rate.

To obtain the initial shock wave development rate shown in figure 4 we require

$$\left[\frac{d}{dx}\log\left(\frac{\Gamma_{\max}-\Gamma_{\max\infty}}{\Gamma_0-\Gamma_{\max\infty}}\right)\right]_0 = -\frac{1}{x_{\beta 0}}. \tag{A 9}$$

Near the origin $\Gamma_{\max} = \Gamma_\alpha$ and $\Gamma_{\max\,\infty}$ is obtained from the structure of the final wave at infinity. In fact the only difference between $x_{\alpha 0}$ and $x_{\beta 0}$ is due to the different aspects of the final wave which need to be considered.

At the piston the initial gradient of $\Gamma_P \equiv \bar{\sigma}_P - \sigma_P$ accurately determines the exponential approach to thermodynamic equilibrium. The characteristic time scale for this approach is $t_P = t_{P0}$, where

$$\left[\frac{d}{dt}\log\left(\frac{\Gamma_P}{\Gamma_0}\right)\right]_0 = -\frac{1}{t_{P0}} = \frac{1}{\Gamma_0}\left(\frac{d\Gamma_P}{dt}\right)_0. \tag{A 10}$$

Now
$$\left(\frac{d\Gamma_P}{dt}\right)_0 = c_{\mathrm{vib}} u_P \left(\frac{dT}{dx}\right)_{P0} - \rho_0 \Gamma_0 \tag{A 11}$$

and along a particle path, using (17) and (18),

$$\frac{dT}{T} = \frac{\gamma-1}{\gamma}\frac{dp}{p} - \frac{\gamma-1}{\gamma T}d\sigma.$$

Hence
$$\frac{dT}{T} = \frac{\gamma-1}{\gamma}\frac{dp}{p} - \frac{(\gamma-1)\rho\Gamma\,dx}{\gamma T u}$$

along the piston path. At the origin

$$\left(\frac{dT}{dx}\right)_{P0} = \frac{\gamma-1}{\gamma\rho_0}\left(\frac{dp}{dx}\right)_{P0} - \frac{(\gamma-1)\rho_0\Gamma_0}{\gamma u_P}. \tag{A 12}$$

Using (A 12) and (A 6), (A 11) becomes

$$\left(\frac{d\Gamma_P}{dt}\right)_0 = -\rho_0\Gamma_0\left\{1+\frac{\gamma-1}{\gamma}c_{\mathrm{vib}}\left[1+\frac{\gamma-1}{1+\dfrac{\rho_0 a_0^2}{(u_{S0}-u_P)\,(dp/du)_{u=u_P}}}\right]\right\},$$

i.e.

$$\left[\frac{d}{dt}\log\left(\frac{\Gamma_P}{\Gamma_0}\right)\right]_0 = -\frac{1}{t_{P0}} = -\rho_0\left\{1+\frac{\gamma-1}{\gamma}c_{\mathrm{vib}}\left[1+\frac{\gamma-1}{1+\dfrac{\rho_0 a_0^2}{(u_{S0}-u_P)\,(dp/du)_{u=u_P}}}\right]\right\}, \tag{A 13}$$

which gives the characteristic time for approach to equilibrium along the piston path.

In the acoustic limit of small piston velocity ($u_P \ll 1$), the right-hand sides of (A 8) and (A 13) become independent of u_P. As $u_P \to 0$, $p_0, \rho_0 \to 1$, $a_0, u_{S0} \to \gamma^{\frac{1}{2}}$ and $(dp/du)_{u_P} \to \gamma^{\frac{1}{2}}$. Hence

$$\left[\frac{d}{dx}\left(\log\frac{\Gamma_\alpha}{\Gamma_0}\right)\right]_{0,\,u_P=0} = -\frac{c_{\mathrm{vib}}(\gamma-1)^2}{2\gamma^{\frac{3}{2}}} = -\frac{1}{x_{\alpha l}} \tag{A 14}$$

and
$$\left[\frac{d}{dt}\left(\log\frac{\Gamma_P}{\Gamma_0}\right)\right]_{0,\,u_P=0} = -\left[1+\frac{\gamma^2-1}{2\gamma}c_{\mathrm{vib}}\right]. \tag{A 15}$$

$x_{\alpha l}$ is used to normalize the decay and development distances x_α and x_β which we obtained from the full characteristics results.

REFERENCES

BLYTHE, P. A. 1969 Nonlinear wave propagation in a relaxing gas. *J. Fluid Mech.* **37**, 31.

CLARKE, J. F. 1960 The linearized flow of a dissociating gas. *J. Fluid Mech.* **7**, 529.

HODGSON, J. P. & JOHANNESEN, N. H. 1971 Real-gas effects in very weak shock waves in the atmosphere and the structure of sonic bangs. *J. Fluid Mech.* **50**, 17.

HORNBY, R. P. & JOHANNESEN, N. H. 1975 The development of weak waves in the steady two-dimensional flow of a gas with vibrational relaxation past a thin wedge. *J. Fluid Mech.* **69**, 109.

JOHANNESEN, N. H., BIRD, G. A. & ZIENKIEWICZ, H. K. 1967 Theoretical and experimental investigation of the reflexion of normal shock waves with vibrational relaxation. *J. Fluid Mech.* **30**, 51.

LICK, W. 1967 Wave propagation in real gases. *Adv. in Appl. Mech.* **10**, 1.

LIGHTHILL, M. J. 1956 Viscosity effects in sound waves of finite amplitude. In *Surveys in Mechanics* (ed. Batchelor & Davies), pp. 250–351. Cambridge University Press.

MOORE, F. K. & GIBSON, W. E. 1960 Propagation of weak disturbances in a gas subject to relaxation effects. *J.A.S.S.* **27**, 117.

OCKENDON, H. & SPENCE, D. A. 1969 Non-linear wave propagation in a relaxing gas. *J. Fluid Mech.* **39**, 329.

SEDNEY, R. 1970 The method of characteristics. In *Nonequilibrium Flows*, part 2 (ed. Wegener), pp. 160–225. Dekker.

ZHUKOV, A. I. 1960 Application of the characteristics method to numerical solution of uni-dimensional problems in gas dynamics. *N.A.S.A. Trans.* (1967) TT-F-298.